Received: 18 November 2020 | Revised: 12 February 2021 | Accepted: 16 February 2021

DOI: 10.1002/navi.416

ORIGINAL ARTICLE

WILEY ION

Precise real-time navigation of LEO satellites using GNSS broadcast ephemerides

André Hauschild | **Oliver Montenbruck**

Deutsches Zentrum für Luft- und Raumfahrt (DLR), German Space Operations Center (GSOC), Weßling 82234, Germany

Correspondence
André Hauschild, DLR/GSOC, Münchener Str. 20, 82234 Weßling, Germany.
Email: andre.hauschild@dlr.de

Abstract

The availability of orbit information with high precision and low latency is a key requirement for many Earth-observation missions, predominantly in the field of radio occultation. Traditionally, precise orbit determination solutions of low-Earth orbit (LEO) satellites are obtained offline on ground after downloading GNSS measurements and auxiliary spacecraft data to the processing center. The latency of this processing depends on the frequency of LEO downlink contacts and the availability of precise GNSS orbit and clock products required for the orbit determination process. These dependencies can be removed by computing the precise orbit determination solution on board the satellite using GNSS broadcast ephemerides. In this study, both real data and simulated measurements from a representative LEO satellite are processed in a flight-proven Kalman-filter algorithm. The paper studies the use of GPS, Galileo and BeiDou-3 for real-time orbit determination in different combinations with simulated measurements. Results show that use of dual-frequency observations and broadcast ephemerides of Galileo and BeiDou-3 leads to a significant reduction of 3D rms orbit errors compared to GPS-only processing. An onboard navigation accuracy of about one decimeter can be achieved without external augmentation data, which opens up new prospects for conducting relevant parts of the science data processing in future space missions directly on board a LEO satellite.

KEYWORDS

broadast ephemerides, precise orbit determination, real-time navigation, signal-in-space range error

1 | INTRODUCTION

Earth-observation missions in low Earth orbit (LEO) commonly rely on the high-precision orbit information to fulfill their scientific objectives. Aside from precision, a low latency of the orbit determination process has become a key requirement, particularly in the field of GNSS radio occultation processing. Here, the velocity of the LEO satellite must be known with a representative accuracy of 0.05 to 0.2 mm/s (corresponding to a position uncertainty of less than 5 to 20 cm) to enable a proper recovery of the tropospheric bending angle and refractivity (Kursinski et al., 1997). The orbit determination as well as the radio occultation data processing must be performed in near-real time (NRT) to allow use of the resulting data in near-term weather forecast (Anthes, 2011). An increasing timeliness

of precise orbit information is also desired in altimetry missions such as Sentinel-3 or Jason-1/2/CS, which aim at determination of the orbit height with few centimeter accuracy in less than a few hours (Desai & Haines, 2010; Roselló et al., 2012).

Dual-frequency GPS or GNSS measurements from receivers on board LEO satellites are routinely used today for precise orbit determination (POD) in a ground-based processing. With the ever improving availability of precise GNSS orbit and clock products in (near-) real time (Agrotis et al., 2017; Kechine et al., 2004), the overall latency of a NRT POD is largely driven by the time to download the GNSS measurements and attitude information of the LEO satellite and to make these data available for processing. Representative NRT POD processes for selected radio occultation and altimetry missions are described in Andres et al. (2010) and Desai and Haines (2010)

As an alternative to traditional ground-based processing, onboard orbit determination may be considered to further reduce the overall latency in the provision of precise orbit information. For many years, this concept has successfully been implemented in the Doppler Orbitography and Radiopositioning Integrated by Satellite (DORIS) Immediate Orbit DEtermination (DIODE) system. Making use of Doppler measurements from a global network of ground beacons, real-time orbit determination solutions with errors of less than 30 cm (3D) and 8 cm (radial) have been achieved with DIODE on various remote sensing missions (Jayles et al., 2010). However, less favorable results with meter-level 3D errors were obtained in most studies and flight trials of onboard orbit determination using unaugmented GPS due to the limited quality of its broadcast ephemerides (Gong et al., 2019; Montenbruck et al., 2008; Reichert et al., 2002; Wang et al., 2015).

To cope with this limitation in GPS-based onboard POD, the transmission of precise GNSS orbit and clock information via a geostationary satellite link has already been proposed almost two decades ago (Reichert et al., 2002; Toral et al., 2006), but not been demonstrated in actual space missions so far. In a more recent study, Hauschild et al. (2016) assessed the use of real-time GPS orbit and clock corrections transmitted through multiple INMARSAT satellites by a commercial service provider. Despite obvious coverage gaps near the poles such real-time corrections can enable real-time positioning with 3D rms errors of less than 9 cm in a reduced-dynamic onboard orbit determination. Alternative (and freely available) systems for dissemination of GNSS orbit and correction data to LEO satellites include satellite-based augmentation systems (SBAS) as proposed in Kim and Kim (2018) or the upcoming Galileo High Accuracy Service (HAS; Fernandez-Hernandez et al., 2018). The latter will offer fully global coverage and can thus support even purely kinematic precise point positioning (PPP). While the actual HAS performance is not presently known, precise orbit and clock corrections similar to those produced by the real-time service (Agrotis et al., 2017) of the International GNSS Service (IGS; Johnston et al., 2017) from a large global network could enable real-time PPP of LEO satellites with 23 cm accuracy (Giordano et al., 2017).

Despite the potential benefit of real-time correction services for GNSS-based onboard navigation, the reception of such correction data on a LEO satellite remains a technical challenge and complexity that has received only limited attention, so far. In particular, this applies for space-qualified L-band or S-band modems (Heckler et al., 2016) to receive corrections from geostationary satellites over a wide range of Doppler shifts, but likewise holds for spaceborne GNSS receivers supporting Galileo E6 tracking and extraction of the HAS data stream.

In the interest of a technically lean solution for GNSS-based onboard navigation we revisit the use of broadcast ephemerides as the sole source of GNSS orbit and clock information of precise real-time orbit determination. With the completion of new GNSS constellations such as Galileo and BeiDou-3 and the continuing progress in GPS modernization, a significant reduction of orbit and clock errors in the broadcast ephemerides can be observed. A superior quality can, in particular, be noted for broadcast ephemerides of the Galileo constellation (Hadas et al., 2019), which offers orbit and clock errors at the 10 to 20 cm level. This makes Galileo a highly promising candidate for precise real-time positioning with broadcast ephemerides and may render the upload of precise corrections obsolete in many applications.

Our study starts with the analysis of broadcast ephemeris errors taking into account modernized navigation messages and the specific aspects of carrier-phase-based positioning (Sect. 2). In the absence of LEO missions with multi-GNSS receivers tracking all relevant constellations, we assess GPS-only real-time POD with broadcast ephemerides for a representative space mission and complement it with use of simulated GNSS measurements of GPS, Galileo, and BeiDou for the same spacecraft and data arc. The Swarm mission used as basis for this analysis is briefly introduced in Sect. 3. The simulation concept and the employed models are described in Sect. 4 before discussing the real-time navigation filter concept and the strategies for handling of broadcast ephemeris errors in Sect. 5. Finally, the achieved orbit determination results for real GPS measurements and simulated multi-GNSS observations are presented and discussed in Sect. 6. This paper is an extension of a previous study with significantly enhanced measurement simulation and navigation filter settings (Hauschild & Montenbruck, 2020).

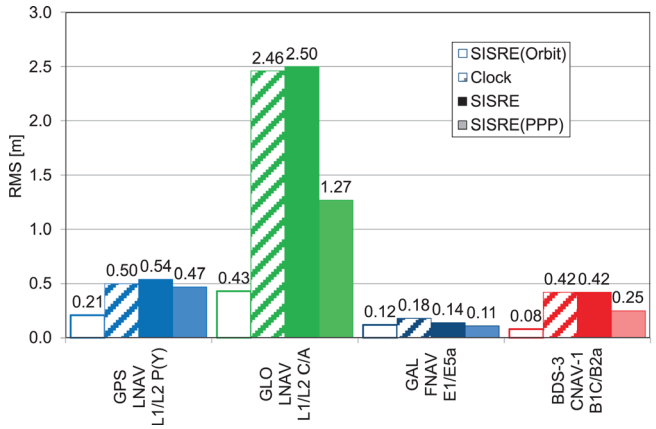

FIGURE 1 RMS signal-in-space range errors of GPS, GLONASS, Galileo, and BeiDou-3 broadcast ephemerides in September 2020 [Color figure can be viewed in the online issue, which is available at wileyonlinelibrary.com and www.ion.org]

2 | BROADCAST EPHEMERIS CHARACTERIZATION

The quality of broadcast ephemeris errors is commonly characterized by the signal-in-space range error (SISRE; Montenbruck et al., 2018b). It provides a measure for the combined effect of clock offset errors and the projection of orbit errors on the line-of-sight vector. The SISRE thus characterizes the error component induced by imperfect GNSS ephemerides in the user's modeled range and, for a given satellite geometry, on the position estimates.

Over the past decade, GPS has experienced a factor-of-two improvement from SISRE values of about 1 m (Gruber, 2010) down to roughly 0.5 m (Haddad et al., 2020) as a result of the ongoing modernization and deployment of highly-stable onboard clocks. Current SISRE statistics for the four global navigation satellite systems GPS, GLONASS, Galileo, and BeiDou-3 are depicted in Figure 1, which shows representative root-mean-square (rms) values of projected orbit errors, clock errors and global-average SISRE errors. These have been computed with respect to a precise reference product of the IGS using the methodology described in (Montenbruck et al. 2018b) and take into account the impact of broadcast group delay errors for dual-frequency users.

For GPS, use of the legacy navigation message (LNAV) and tracking of the P(Y)-code on L1/L2 have been assumed for the SISRE analysis, since modernized civil navigation signals and messages are presently only available for a subset of the full constellation. However, only marginal differences are obtained for the new civil navigation message (CNAV) SISRE and use of L1 C/A plus L2C or L5 observations, since LNAV and CNAV are derived from the same orbit and clock determination process and have similar upload intervals (Haddad et al., 2020).

GLONASS results apply for use of the FDMA navigation message and tracking of the public C/A-code signal on L1 and L2, while use of the FNAV message and E1/E5a open signal tracking is considered for Galileo. Finally, use of the modernized civil navigation message (CNAV-1) and tracking of the interoperable B1C and B2a signals is assumed in the BeiDou-3 SISRE analysis. Furthermore, only satellites in medium Earth orbit (MEO) have been considered for this constellation in view of their global coverage.

Notable differences among the four constellations are obvious and a performance benefit over the legacy constellations may be recognized for the two new GNSSs, Galileo and BeiDou-3. Clock errors are typically larger than the projected orbit errors and thus the dominant contributor to the SISRE. This is especially pronounced for GLONASS, which exhibits the largest rms SISRE of 2.5 m, but also for GPS and BeiDou-3 with SISREs of 0.54 m and 0.42 m, respectively. An exceptionally low SISRE of 0.14 m is achieved by Galileo, which benefits from the use of highly stable passive hydrogen masers on most satellites of the constellation and a short, 10 to 100 min, update cycle of its broadcast ephemerides.

While SISRE provides a well-established figure of merit for pseudorange-based single-point positioning (SPP) it may not be fully representative for carrier-phase-based PPP techniques. Typically, the comparison of broadcast and precise ephemerides is contaminated by satellite-specific clock offsets that can be attributed to inconsistent group delays in the determination of the respective clock products. While clearly relevant for pseudorange-based positioning, such inconsistencies are largely lumped into the estimated carrier phase ambiguity in precise point positioning or orbit determination. We therefore complement Figure 1 by a specific "PPP-SISRE" in which satellite-specific, but constant biases have been removed in the clock comparison on a daily basis. In the period covered by Figure 1, such biases had RMS values of 0.26 m, 2.30 m, 0.11 m, and 0.35 m for satellites of the GPS, GLONASS, Galileo, and BeiDou-3 constellation, respectively. When excluding these contributions in the SISRE evaluation a smaller SISRE for all constellations, and now reveals a clear performance merit for both BeiDou-3 (0.25 m) and Galileo (0.10 m) in carrier-phase based positioning. Both constellations thus offer the best prospects for unaugmented, carrier-phase-based real-time navigation of LEO satellites and represent the focus of our study.

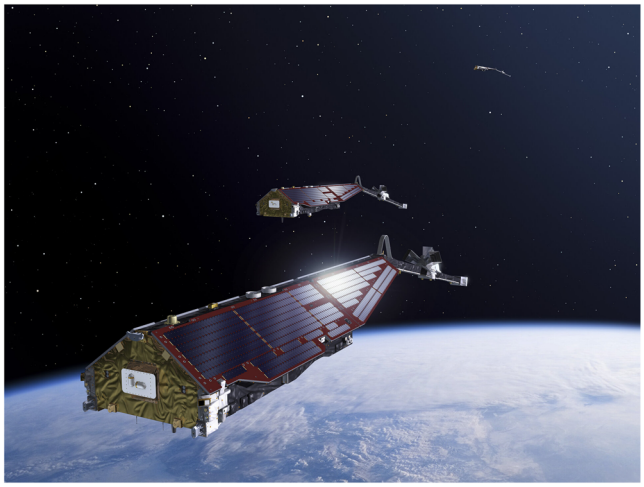

FIGURE 2 Artist's impression of the three original Swarm satellites. The booms point in the anti-flight direction. The two GPS antennas are mounted on the top side and nominally point towards zenith (image: ESA-P.Carril) [Color figure can be viewed in the online issue, which is available at wileyonlinelibrary.com and www.ion.org]

3 | EXAMPLE LEO SATELLITE MISSION AND TEST DATA

For this study, real-time onboard POD is assessed using true and simulated GNSS observations of the Swarm-C satellite (Figure 2), which is considered representative in terms of orbit and attitude for many Earth-observation missions. It was launched on November 22, 2013, and is part of an initial constellation of three identical satellites that serves to characterize Earth's magnetic and electric fields. Swarm-C orbits the Earth in roughly 93 minutes on a polar orbit with 87.4° inclination at an altitude of about 440 km (in 2020).

Each Swarm satellite is equipped with a cold-redundant pair of RUAG GPSR dual-frequency GPS receivers (Zangerl et al., 2014) and zenith-pointing Patch Excited Cup (PEC) antennas (Wettergren et al., 2009). The GPSR receiver tracks the GPS L1 C/A and L1/L2 P(Y) signals for up to eight satellites, and provides measurements of pseudorange, carrier-phase, Doppler and C/N_0. These are used to obtain precise science orbits (PSOs) of the Swarm satellite in a reduced dynamics orbit determination (van den IJssel et al., 2015). Previous studies have shown that these orbits have an accuracy on the order of a few centimeters (Montenbruck et al., 2018a).

A 24-hour set of flight data for September 15, 2020, has been selected as the basis for this study. It comprises dual-frequency GPS measurements of the GPSR instrument as well as precise science orbits, attitude quaternions and auxiliary information about the satellite's mass, center-of-mass and antenna position made available at (ESA, 2020).

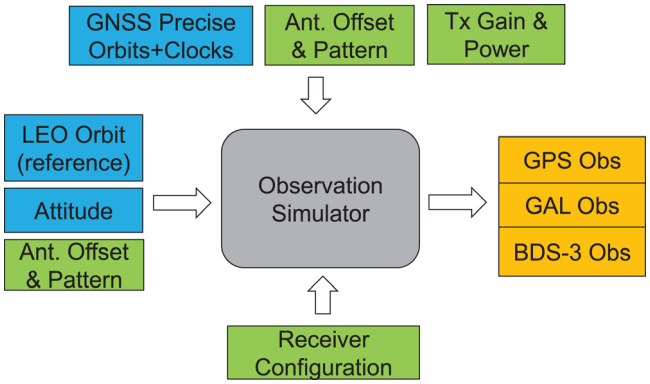

FIGURE 3 Simulation of multi-GNSS observations for spaceborne receivers. Individual colors indicate time varying motion and clock data (blue), static configuration parameters (green) and output data (orange) [Color figure can be viewed in the online issue, which is available at wileyonlinelibrary.com and www.ion.org]

In addition to the real flight data, simulated measurements for GPS, Galileo, and BeiDou have been generated with a GNSS measurement simulation software, which will be described in the following section.

4 | MULTI-GNSS MEASUREMENT SIMULATION FOR SPACEBORNE RECEIVERS

For best compatibility of real and simulated Swarm GNSS observations, a software-based, measurement-level simulation approach (Petovello & Curran, 2017) has been adopted in our study. It is limited to offline simulations, but enables full control of all simulation models and does not suffer from corresponding restrictions of common GNSS radio-frequency signal simulators. A conceptual view of the Observation SImulation of Receivers In Space (OSIRIS) software is shown in Figure 3. Based on the reference orbit and attitude for the Swarm satellite as well as a precise orbit and clock product for the GPS, Galileo and BeiDou constellations, dual-frequency pseudorange, carrier-phase, Doppler and C/N_0 measurements were simulated for the day of interest and output in the Receiver Independent Exchange (RINEX; IGS/RTCM, 2019) format for further processing.

Specific models and configuration parameters employed in the simulation are summarized in Table 1. The center-of-mass trajectory of the LEO satellite as well as the instantaneous attitude, which is used to model the antenna position, are described through precise orbit and attitude products from the Swarm science data archive. Likewise, GNSS orbits and clock offsets are described through a precise multi-GNSS ephemeris product provided by one of the IGS analysis centers. The received signal strength and the

TABLE 1 Models and parameters for Swarm multi-GNSS observation simulation. Individual signals are identified by RINEX (IGS/RTCM, 2019) observation codes

Item	Description
GNSS constellation	
Orbits and clock offsets	GFZ0MGXRAP rapid multi-GNSS product with 5 m orbit and 30 s clock sampling (CDDIS, 2020)
Attitude	Models of rate-limited yaw-steering (Dilssner, 2010; Dilssner et al., 2018; GSC, 2019; Kouba, 2009)
Antenna offsets & phase variations	igs14.atx (week 2118)
Code biases	CAS0MGRAP differential code bias product (CDDIS, 2020)
LEO satellite	
Spacecraft center of mass	Swarm-C precise science orbit (ESA, 2020)
Attitude	Star sensor based attitude quaternions (ESA, 2020)
Center of mass	(-1.9540 m, +0.0010 m, -0.3340 m) ESA (2020)
Antenna reference point	(-1.6502 m, +0.0010 m, -0.8055 m) ESA (2020)
Link model	
GNSS gain patterns	Marquis and Reigh (2015), Monjas et al. (2010), Valle et al. (2006), Zhan et al. (2013)
Transmit power	Steigenberger et al. (2018), Steigenberger et al. (2019)
Receiver antenna gain pattern	RUAG PEC antenna (Wettergren et al., 2009)
Losses	4.5 dB for LNA noise figure and A/D conversion losses (Moreau et al., 2002)
Receiver model	
Clock	Linear drift, controlled within ±0.5 ms
Channels	2×8 per constellation (GPS, Galileo, BeiDou-3)
Signals	GPS: semi-codeless P(Y) (1W, 2W), or L1 C/A + L2C (1C, 2L), or L1 C/A + L5 pilot (1C, 5Q)
	GAL: E1 O/S & E5a pilot (1C, 5Q)
	BDS-3: B1C & B2a pilot (1P, 5P)
Early-late correlator spacing	GPS 1C: 0.14 chips; GPS 1W, 2W: 0.5 chips; GPS 2L: 0.28 chips; GAL 1C, BDS-3 1P: 0.07 chips; GPS 5Q, GAL 5Q, BDS-3 5P: 0.7 chips
DLL bandwidth	GPS 1W, 2W: 0.10 Hz; GPS 2L: 0.25 Hz; GPS 5Q, GAL 5Q, BDS-3 5P: 1 Hz; others 0.5 Hz
PLL bandwidth	GPS 1W, 2W: 1 Hz; others: 15 Hz
Elevation mask	0°
Acquisition/tracking threshold	15 dBHz / 10 dBHz for GPS P(Y), all others 35 dBHz / 30 dBHz
Observation model	
Light-time	Modeled (iterative solution)
Relativity	Modeled (periodic clock variation, Shapiro effect)
Phase wind-up	Modeled (Wu et al., 1993)
Ionospheric path delay	Constant vertical TEC (10 TECU) and thick-layer mapping function (Lear, 1989)
Receiver antenna phase center offset	Zero (GPS L1/L2 offset included in antenna reference point; same value assumed for other signals)
Receiver antenna phase variations	GPS L1/L2 phase variations from in-flight calibration; applied for all signals
Receiver antenna multipath	Phase multipath included in phase pattern; in-flight calibration of GPS L1 and L2 pseudorange multipath applied for signals in L1/E1/B1 and L2/E5a/B2a frequency bands, respectively

resulting C/N_0 are modeled based on GNSS transmit power values, as well as transmit and receiver antenna gains, taking into account free-space losses and additional receiver-specific implementation losses (Moreau et al., 2002). In case of incomplete parameters for some constellations or signals, the respective values were obtained by adjusting the resulting C/N_0 to representative ground receiver measurements.

Error-free pseudorange, carrier phase, and Doppler values are first computed based on the known transmitter/receiver antenna geometry and clock offsets using established PPP models (Hauschild, 2017). Subsequently, measurements noise is added based on the modeled C/N_0 for configurable receiver characteristics and the specific properties of each individual signal (Betz, 2016). Key receiver parameters for the noise model comprise the bandwidths of the delay lock loop (DLL) and phase lock

loop (PLL) as well as the early-minus-late correlator spacing. For semi-codeless tracking of the encrypted GPS P(Y)-code, characteristics of the Z-tracking technique (Woo, 2000) are assumed in the corresponding C/N_0 and noise model. Individual receiver settings are selected to mimic the performance of the Swarm GPSR receiver and RUAG's next-generation GPS/Galileo receiver (PODRIX) that will be flown on the next batch of Sentinel-1/2/3 satellites and the Sentinel-6/Jason-CS mission. In view of similar signal properties, matching tracking parameters were assumed for corresponding BDS-3 and Galileo signals on the E1/B1 and E5a/B2a frequencies.

Next to receiver noise, receiver antenna phase pattern distortions and multipath errors are considered in the simulation. For LEO satellites without moving appendices, multipath for a given signal depends only on the line-of-sight direction and can thus be described by a static correction function in terms of azimuth and elevation angle of the tracked satellite in the antenna diagram. The combined effect of antenna patterns and multipath can thus be described through code and multipath maps. Examples for the Swarm satellites as derived from in-flight calibrations are given in van den (IJssel et al. 2015) and (Mao et al. 2018). Representative amplitudes range from 0.1 to 0.2 m and 2 to 3 mm for single-frequency pseudorange and carrier-phase observations, respectively, and roughly 3-times higher values apply for the ionosphere-free dual-frequency combination.

For the present study, P(Y)-code signals on L1 (1575.420 MHz) and L2 (1227.600 MHz) were simulated for a total of 30 healthy GPS satellites. For an assessment of modernized open service signals, independent simulations were performed assuming a receiver configured for L1 C/A and L2C tracking of the sub-constellation of 21 Block IIR-M, Block IIF, and GPS III satellites, and a receiver configured for L1 C/A and L5 tracking of the 14 healthy Block IIF and GPS III satellites available at the time of interest. While the latter configuration would hardly be useful for standalone navigation, the signals are fully interoperable with other GNSSs and would be of interest for mixed GPS/Galileo or GPS/BeiDou operation. Also, L2C and L5 offer access to the new civil navigation message (CNAV), which includes both group delay and Earth orientation information for real-time navigation users.

In the case of Galileo, E1B (1575.420 MHz) and E5a (1176.450 MHz) pilot signals were simulated for the entire set of 24 satellites transmitting these signals on the day of interest, including the two satellites injected into eccentric orbits. In the case of BeiDou-3, the B1C (1575.420 MHz) and B2a (1176.450 MHz) pilot signals were modeled for the full set of 24 MEO satellites in the constellation. The overall number of visible satellites in the field of view is typically larger than the assumed number of dual-frequency

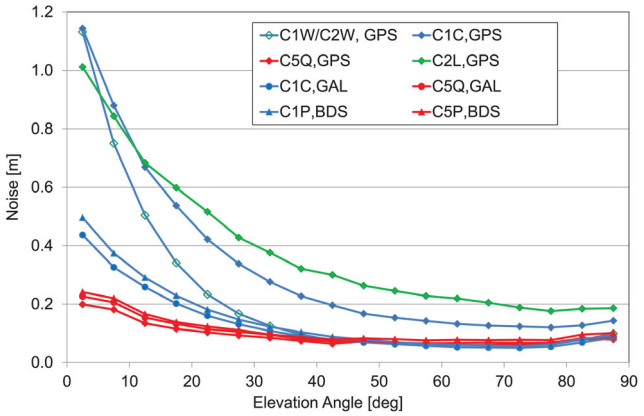

FIGURE 4 Pseudorange noise and multipath (standard deviation) over elevation angle for the simulated GPS, Galileo, and BeiDou-3 measurements. A small increase at very high elevation angles is related to antenna group delay distortions observed near the bore sight direction [Color figure can be viewed in the online issue, which is available at wileyonlinelibrary.com and www.ion.org]

channels. As a result, the tracking channels are fully used for most of all epochs and an average of 7 to 8 each of the GPS, Galileo, BeiDou-3 satellites were tracked in the simulation.

The magnitude of the combined noise and multipath errors of the simulated pseudorange observations over elevation angle is illustrated in Figure 4. The largest errors are obtained for the legacy GPS L1 C/A-code as well as the L2C-code which use a traditional binary phase shift keying (BPSK) modulation and a roughly 300 m chip length. The GPS L1/L2 P(Y) pseudorange observations benefit from a ten-times smaller chip length, but exhibit increased noise at low elevation angles due to the inherent semi-codeless tracking losses. Compared to the legacy GPS signals, a clearly improved performance is obtained for the E1/B1 signals of the new constellations. Among others, tracking of these signals benefits from the binary-offset-carrier (BOC) modulation, which allow for a 3-times lower noise variance than traditional binary phase shift keying (BPSK) signals at the same loop bandwidth. With values of less than 20 cm even down to the horizon, the lowest pseudorange noise is obtained for the GPS L5, Galileo E5a and BeiDou-3 B2a signals that benefit from both a high signal power and a 10-times lower chip length than other open service signals. In addition to the low SISRE of Galileo and BeiDou-3, these constellations also provide a favorable measurement quality, which is again considered beneficial for positioning performance. The small increase of the noise at very high elevation angles is related to antenna group delay distortions near bore-sight direction.

The average magnitude of pseudorange and carrier-phase errors for the true GPS measurements of Swarm

TABLE 2 RMS noise and multipath of real and simulated GNSS measurements. All values apply for the ionosphere-free dual-frequency combination

		Noise		Noise+MP	
GNSS	**Signals**	**[m]**	**[mm]**	**[m]**	**[mm]**
GPS (true)	L1/L2 P(Y)	–	–	0.80	6.6
GPS (sim)	L1/L2 P(Y)	0.77	5.1	0.79	7.1
	L1CA/L2C	1.52	3.4	1.54	6.5
	L1CA /L5	1.13	2.5	1.14	5.8
GAL (sim)	E1/E5a	0.45	2.5	0.48	6.1
BDS-3 (sim)	B1C/B2a	0.47	2.7	0.50	6.2

and the simulated observations as derived from POD residuals with and without antenna pattern corrections is summarized in Table 2. For GPS, the simulated P(Y) measurements closely match those of the real Swarm observations in terms of pseudorange noise and outperform L1 C/A and L2C. Simulated observations for Galileo and BeiDou-3 have 30 to 50% smaller pseudorange errors than for GPS P(Y) tracking, which reflects the improved properties of open dual-frequency signals for these constellations. For phase errors, only small differences apply for the individual observation types and constellations due to the dominating contribution of multipath errors in the simulation. The average pseudorange errors, on the other hand, are dominated by receiver noise.

5 | ONBOARD REAL-TIME PRECISE ORBIT DETERMINATION

The on-board LEO POD performance using multi-GNSS observations and broadcast ephemerides is assessed with a Kalman-filter-based real-time navigation algorithm, which has been developed for use in spaceborne GNSS receivers and on board navigation systems (Montenbruck & Ramos-Bosch, 2008). Aside from its use for concept studies of real-time navigation, the algorithm has flight heritage through the Phoenix eXtended Navigation System (XNS) onboard the PROBA-2 microsatellite (Montenbruck et al., 2008).

The filter is capable of processing single- or dual-frequency measurements and can be used with pseudoranges only or with both pseudorange and carrier-phase measurements. In the configuration used for this study, the algorithm processes dual-frequency pseudorange and carrier-phase GNSS observations of one or multiple constellations. Although the data are processed offline in the present context, the algorithm emulates a *true* real-time process. It employs a sequential estimator operated in forward mode and uses only past and current observations in the data cleaning and quality control.

In addition to the LEO satellite's position ($\boldsymbol{r}$) and velocity ($\boldsymbol{v}$), the filter's state vector

$$\boldsymbol{y} = (\boldsymbol{r}; \boldsymbol{v}; C_\mathrm{D}; C_\mathrm{R}; \boldsymbol{a}_\mathrm{emp}; c\delta t_1; \ldots; c\delta t_m; A_1; \ldots; A_n) \quad (1)$$

comprises 5 dynamical model parameters including scaling coefficients for atmospheric drag (C_D) and solar radiation pressure (C_R), as well as a vector $\boldsymbol{a}_\mathrm{emp} = (a_\mathrm{R}, a_\mathrm{A}, a_\mathrm{C})$ of empirical accelerations in radial-, along- and cross-track directions. For each of the m constellations handled by the navigation filter, a distinct receiver time offset $c\delta t_i$ ($i = 1, \ldots, m$) is considered in the state vector. Finally, a carrier-phase ambiguity A_j ($j = 1, \ldots, n$) is estimated for each of a total n tracked satellites.

The prediction model for the satellite trajectory takes into account accelerations due to Earth's gravity field, luni-solar-perturbations, drag, solar-radiation pressure, and empirical accelerations. An Earth-fixed formulation of the equation of motion is used, which avoids the need for explicit reference system transformations in the observation model and requires only low-precision transformations for obtaining Earth-fixed coordinates of the Sun and Moon. Nevertheless, proper knowledge of Earth-orientation parameters (EOPs) is still required for the instantaneous Earth rotation vector in the modeling of Coriolis and centrifugal accelerations (Montenbruck & Ramos-Bosch, 2008). Predicted EOPs are presently made available in the modernized navigation messages of GPS and BeiDou-3 with a representative accuracy of 0.001″ for pole coordinates and 0.001 s for the UT1−UTC time difference. For the present study, EOPs from the GPS CNAV message were used. Given the low altitude of Swarm, an Earth gravity model of order and degree 70 is typically required for precise orbit determination at the (sub-) decimeter level and was also adopted here for the real-time navigation process.

If necessary, biases in the pseudorange observations have been corrected for by Timing Group Delays (TGD) and Inter-Signal Corrections (ISCs) for GPS and Beidou-3 as well the Broadcast Group Delays (BGDs) for Galileo from the broadcast ephemerides of the respective navigation systems. In the simulation of the measurements, estimated code biases from a precise reference product of the Chinese Academy of Sciences (CAS) have been used. Science the broadcast values are provided by the GNSS ground segment and the CAS biases have been estimated from a geodetic reference receiver network, the differences introduce realistic residual pseudorange modeling errors in the processing.

Within the extended Kalman filter, the scaling parameters for drag and solar radiation are treated as random walk parameters. They are propagated as constant values but white process noise is added to the covariance to allow

TABLE 3 Data, models and algorithms for real-time navigation

Item	Description
Observation model	
Measurement types	Ionosphere-free combination of dual-frequency pseudorange and carrier-phase observations for GPS, Galileo, BeiDou-3
Sampling	30 s
GNSS orbits and clocks	Broadcast ephemerides (GPS: LNAV or CNAV, Galileo: FNAV, BeiDou-3: CNAV-1); periodic relativistic clock correction
Antenna model	Swarm antenna offset and attitude, no phase variations; zero antenna offset for GNSS satellites
Group delays	Satellite TGDs and ISCs (GPS, BeiDou-3) and BGDs (Galileo) from broadcast ephemerides; no receiver group delays
Phase wind-up	neglected
Motion model	
Reference frame	Earth-fixed equation of motion including Coriolis and centrifugal accelerations; IAU 1976 precession, IAU 1980 nutation and sidereal time; GPS CNAV Earth orientation parameters
Earth gravity	GGM01S model (70×70) (Tapley et al., 2004), k_2 tides (Rizos & Stolz, 1985), no relativity
Third-body perturbations	Point-mass model for Sun and Moon; analytical series truncated to $1'$ and $5'$ (Montenbruck & Gill, 2000)
Solar radiation pressure	Cannon-ball model; conical Earth shadow
Drag	Cannon-ball model; static density model for medium-solar flux (Harris & Priester, 1962)
Empirical accelerations	Accelerations in radial, along-track and cross-track direction; piece-wise constant across time update steps
Numerical integration	4th-order Runge-Kutta method with Richardson-extrapolation and 4th-order interpolant (Hairer et al., 1987)
Estimation	
Type	Extended Kalman-filter
State parameters	Position, velocity, drag and radiation pressure scale factors, empirical accelerations, GNSS-specific receiver clock offsets, carrier-phase ambiguities
Stochastic parameters	Random walk model for clock and ambiguities, exponentially correlated random variables for empirical accelerations

for possible variations in time. Empirical accelerations are used to compensate deficiencies in the deterministic force model. They are treated as exponentially correlated random variables with zero mean value and configurable correlation time τ and steady-state standard deviation $\sigma_{a_{R,A,C}}$.

To facilitate use of the real-time navigation algorithm with a wide range of receiver clock types including both steered and free-running oscillators, the constellation-specific receiver clock offsets are reinitialized to coarse values obtained from a kinematic navigation fix at each time-update step. Along with a large a priori covariance this enables an essentially free clock offset adjustment in the filter and can even handle millisecond-level clock adjustments as used in many geodetic GNSS receivers.

The Kalman filter and reduced dynamic orbit model are well suited to cope with noisy measurements in the real-time navigation process. However, they only partly "smooth" the contribution of GNSS orbit and clock errors in the range modeling, which results from use of broadcast ephemerides instead of precise GNSS ephemerides. The signal-in-space range error that includes the projection of orbit errors on the line of sight and the GNSS clock offset error is typically characterized by gradual drifts, small stochastic variations, and jumps of varying magnitude at the instant of broadcast ephemeris updates. Due to rapid changes of the line-of-sight vector, variations of the SISRE in time are more rapid for a LEO satellite than for terrestrial users. Typical SISRE rates and discontinuities encountered in practice amount to 0.5 m/h and 0.5 m, respectively for GPS (see, e.g., Gong et al. (2020)), while 2 to 4 times smaller values apply for BeiDou-3 and Galileo.

To cope with broadcast ephemeris errors, a dedicated SISRE state may be introduced for each tracked satellite and estimated along with the other parameters as suggested in (Gunning et al. 2019). While this approach offers a rigorous SISRE handling in both the pseudorange and carrier-phase observation model, it notably increases the state dimension (from $11 + m + n$ to $11 + m + 2n$) and thus the computational burden of each update step. We therefore adopt a simpler but almost equally effective approach, in which the projected orbit errors and clock errors are lumped with the carrier-phase ambiguities (Montenbruck et al., 2008). The resulting

TABLE 4 Kalman-filter parameters and settings for real-time onboard navigation

Parameter		GPS	GPS	GPS	GPS	Galileo	BeiDou-3
Signals		L1 & L2 P(Y)	L1 & L2 P(Y)	C/A & L2C	C/A & L5	E1/E5a	B1C & B2a
Ephemeris		precise	LNAV	CNAV	CNAV	F/NAV	CNAV-1
Weighting							
Pseudorange	σ_{PR}	1.0 m	1.5 m	2.5 m	2.0 m	1.0 m	1.0 m
Carrier phase	σ_{CP}	0.01 m	0.01 m	0.01 m	0.01 m	0.01 m	0.01 m
Process noise							
Emp. accelerations	σ_{a_R}	5 nm/s^2	5 nm/s^2	5 nm/s^2	5 nm/s^2	5 nm/s^2	5 nm/s^2
	σ_{a_A}	10 nm/s^2	20 nm/s^2	20 nm/s^2	20 nm/s^2	20 nm/s^2	20 nm/s^2
	σ_{a_C}	10 nm/s^2	40 nm/s^2	40 nm/s^2	40 nm/s^2	40 nm/s^2	40 nm/s^2
	τ	600 s	600 s	600 s	600 s	600 s	600 s
Clock	$Q_{c\delta t}$	$(500m)^2$	$(500m)^2$	$(500m)^2$	$(500m)^2$	$(500m)^2$	$(500m)^2$
Pseudo-ambiguity	Q_A (at 30 s)	(0 mm)^2	(20 mm)^2	(20 mm)r	(20 mm)r	(5 mm)r	(5 mm)r
Data editing thresholds							
Elevation angle		0°	0°	0°	0°	0°	0°
C/N$_0$		5 dBHz	5 dBHz	5 dBHz	5 dBHz	5 dBHz	5 dBHz

"pseudo-ambiguity" (Wang et al., 2015) can then be estimated as a random-walk parameter by considering white process noise in the time update of this parameter.

Even though the application of appropriate process noise also allows adjusting to SISRE jumps at broadcast ephemeris updates (Gong et al., 2020) in the estimated ambiguities, we prefer to actively account for such discontinuities. When switching to a new set of broadcast ephemerides, as indicated by a change in the issue-of-data counter or the ephemeris epoch, the associated SISRE change is evaluated by comparing the predicted range and clock offset for the old and new ephemeris set at the new measurement epoch and applied as an update to the corresponding pseudo-ambiguity.

For completeness, we note that the concept of pseudo-ambiguities introduces an inconsistency in the filter, since SISRE is only considered in the carrier-phase model but neglected in the pseudorange observation model. However, this inconsistency can well be tolerated in practice and compensated by a modest down-weighting of the pseudorange measurements.

Table 4 summarizes selected configurations and filter parameters for the multi-GNSS real-time Kalman-filter processing. The observation weights adopted in the individual cases are selected based on the magnitude of noise and multipath errors, as well as SISRE for the respective GNSSs. Process noise for the pseudo-ambiguities is based on the previously discussed SISRE properties, taking into account the temporal variation of line-of-sight orbit errors and the stochastic GNSS satellite clock variations. Finally, the process noise parameters for the empirical accelerations are derived from a parametric search for filter tuning. A flat performance minimum with less than 20% variation of the navigation errors can typically be observed when adjusting process noise or weights by up to a factor of two.

For comparison, the first case in Table 4 furthermore specifies filter settings for processing with a precise GPS orbit and clock product. Here, no process noise is applied and tighter constraints for the empirical accelerations are used for best performance. The corresponding filter results are indicative of the LEO navigation performance that might be obtained with real-time correction services (Hauschild et al., 2016) under optimum conditions and will be used as a benchmark for the subsequent analysis of real-time navigation using broadcast ephemerides.

6 | RESULTS AND DISCUSSION

The real-time navigation accuracy of LEO satellites that can be achieved with multi-GNSS observations and broadcast ephemerides has been evaluated using real GPS observations collected onboard the Swarm-C satellite as well as simulated GPS, Galileo, and BeiDou-3 measurements. All tests cover a 24 h period on September 15, 2020, where a total of 30 GPS satellites, 22 Galileo satellites, and 24 BeiDou-3 MEO satellites were declared healthy. Within the GPS constellation, healthy L2C and L5 signals were transmitted by a subset of 21 and 14 satellites, respectively. In the case of Galileo, the two satellites (E14, E18) in eccentric orbits are still marked as unhealthy. Even though their ranging signals are of high quality, their broadcast ephemerides show a slightly degraded performance and the satellites are not included in the Galileo almanac. As such, the tests are limited to a partial Galileo constellation that has not yet achieved full operational capability.

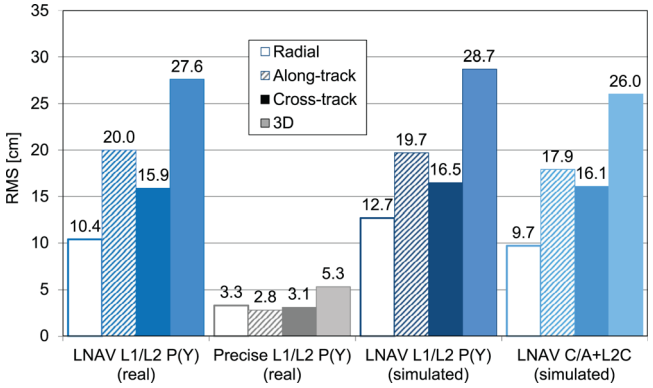

FIGURE 5 Simulated real-time LEO POD errors using real GPS flight data and simulated observations with different sets of orbit and clock information [Color figure can be viewed in the online issue, which is available at wileyonlinelibrary.com and www.ion.org]

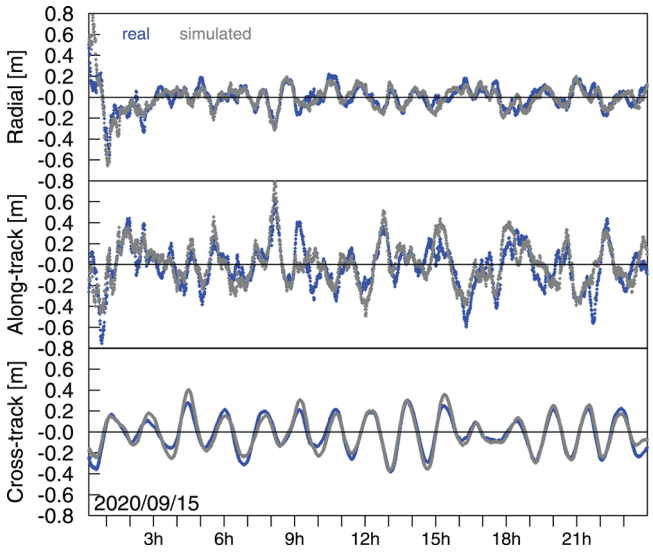

FIGURE 6 Position errors in radial, along-track, and cross-track direction for processing of real Swarm GPS observations (blue) and simulated data (gray) [Color figure can be viewed in the online issue, which is available at wileyonlinelibrary.com and www.ion.org]

Figure 5 shows the results for simulated real-time POD results using real-live and simulated GPS measurements. In all cases, the Swarm-C precise science orbit served as the truth reference for the performance evaluation and a 15 min interval at the beginning of the data arc was discarded to focus on the steady-state performance of the navigation filter.

When working with the legacy navigation message and the real GPS P(Y) observations collected on board Swarm, a 28 cm 3D RMS accuracy is obtained using the filter settings of Table 4. Other than in kinematic position solutions, which suffer from a poor vertical dilution of precision, the vertical component exhibits the least errors. This is of particular interest for altimetry missions and reflects the dynamical constraints provided by a high-fidelity orbit model.

Compared to earlier studies based on similar filter models (Montenbruck et al., 2008, 2013) a 30 to 40% reduction of the position error may be observed, which can essentially be attributed to the improved SISRE and clock stability of the modernized GPS constellation. With these improvements, it may be recognized that a GPS-only navigation filter can now achieve an onboard orbit determination accuracy closely matching that of the DORIS-based DIODE navigation system as reported in Jayles et al. (2010).

To illustrate the impact of broadcast ephemeris uncertainty on the filter performance, the same set of flight data has furthermore been processed using precise GPS orbit and clock data as provided by the IGS. Here, a 5 cm accuracy is achieved. While not necessarily representative for current onboard applications, the test provides a validation of the overall filter design in our study and indicates the performance that could be achievable in onboard navigation systems with high-quality real-time GPS/GNSS correction services.

The third test case shown in Figure 5 is again based on broadcast ephemerides, but now makes use of the simulated GPS P(Y) observations described in Sect. 4. A closely matching overall navigation performance is obtained compared to processing of the real-flight data. This is further illustrated by Figure 6, which shows the evolution of navigation errors in all three axes over time. Even though the simulation cannot exactly replicate the channel allocation of the Swarm-C GPS receiver and exhibits occasional differences in the set of tracked satellites, a high correlation is obvious for the two cases. As such, the test confirms that the observations created by the simulation reflect the quality of the GPS onboard receiver measurements in a realistic manner.

Use of simulated observations allows us to study the potential benefit of using the new civil L2C signal along with the legacy C/A-code on the L1 frequency. Civil users have long been encouraged to transition to these signals for dual-frequency positioning and a growing number of space receivers are supporting these signals as an alternative to semi-codeless P(Y) tracking. The open signals are considered to offer more robust tracking even though their pseudorange noise is typically higher due to the large chip length of the ranging code. Despite the fact that L2C is only transmitted by two-thirds of the current GPS constellation so far, a sufficient number of satellites is typically in the fields of view to exploit the capabilities of an 8-channel (per signal) receiver such as the one used on Swarm.

Overall, the test results in Figure 5 confirm that tracking of the civil L1/L2 signals from the subset of L2C-capable

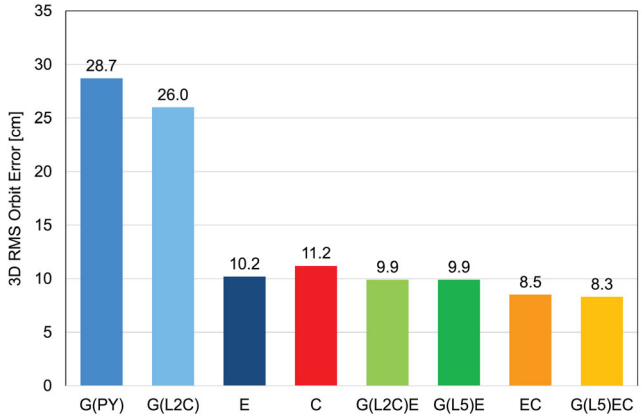

FIGURE 7 Simulated real-time LEO POD 3D rms orbit errors for different combinations of GPS, Galileo and BeiDou-3 data [Color figure can be viewed in the online issue, which is available at wileyonlinelibrary.com and www.ion.org]

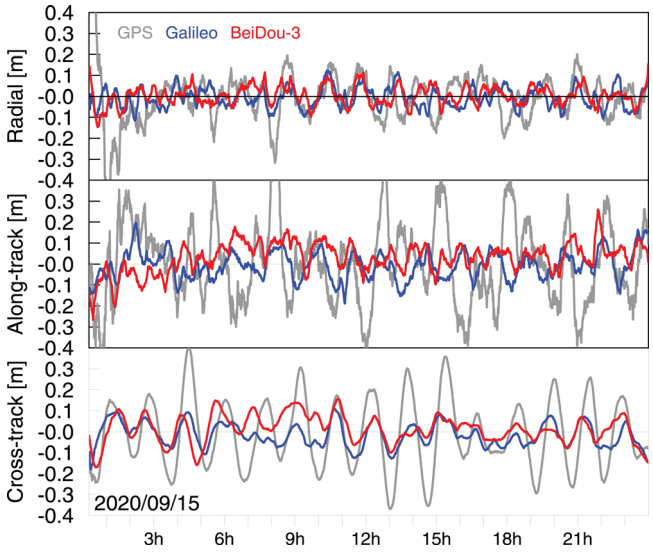

FIGURE 8 Position errors in radial, along-track, and cross-track directions for processing of simulated GPS P(Y) (gray), Galileo E1/E5a (blue), and BeiDou-3 B1C/B2a (red) observation [Color figure can be viewed in the online issue, which is available at wileyonlinelibrary.com and www.ion.org]

GPS satellites and use of the corresponding CNAV message can already offer an almost identical navigation performance as the established use of P(Y) tracking and LNAV. On average, the modernized satellites transmitting L2C even offer a better clock stability and thus slightly better average SISRE than the full constellation, which even allows for a small performance gain of L2C-based navigation in the present study. It is also instructive to note that the increased pseudorange noise of L1 C/A and L2C measurements as compared to P(Y) observations does not affect the overall performance in an adverse manner. This supports the understanding that pseudorange observations have only limited contribution in a reduced-dynamic navigation filter and SISRE is the driving factor for the achievable navigation accuracy.

Results for simulated observations of GPS, Galileo, and BeiDou-3 are summarized in Figure 7. Compared to GPS, standalone Galileo and BeiDou-3 solutions offer a 60% reduction of the navigation errors and achieve a remarkable 3D rms position accuracy close to one decimeter. The notable performance improvement can essentially be attributed to the improved quality of the broadcast ephemerides and largely reflects the PPP-SISRE of the individual constellations (Figure 1). Even though the advanced signal modulations used in the new constellations offer a notably smaller pseudorange noise than those of currently available GPS signals, pseudorange observations have only limited contribution to the filter performance as discussed above. Similar to GPS-based navigation, the radial component of the position vector exhibits the smallest error of all axes (Figure 8) and can be determined with an rms accuracy of 5 cm with either Galileo or BeiDou-3.

With a 3D rms error of only 8.5 cm, optimum dual-constellation results can be obtained by joint Galileo E1/E5a and BeiDou-3 B1C/B2a tracking. Aside from a favorable performance, that comes even close to the ideal case of using precise GNSS ephemerides, the combination is attractive in view of the common frequency bands used by these open service signals. This allows for a lean GNSS receiver design with limited complexity of the radio-frequency front end. Furthermore, the modernized CNAV-1/-2 navigation messages of BeiDou-3 offer EOPs similar to GPS CNAV, thus coping with a limitation of the current Galileo navigation message for spaceborne users.

Given the obvious performance difference between GPS and Galileo/BeiDou-3, a combination of all three systems does not show relevant benefits in terms of accuracy. Unless required for highest robustness and redundancy, the hardware and processing effort for using three constellations does not appear to be justified. In order to illustrate the increase in computational effort, the processing times for one, two and three constellations have been compared. It turns out that the processing time increases by a factor of 5 for dual-constellation and by a factor of 20 for triple-constellation processing. It must be noted, though, that the algorithm has not been optimized for efficient processing.

7 | SUMMARY AND CONCLUSIONS

The study assesses the on-board precise real-time navigation performance that is currently possible with broadcast

ephemerides from GPS as well as Galileo and BeiDou-3. For this purpose, multi-frequency and multi-constellation measurements are simulated for the Swarm-C LEO satellite. The simulated data are processes in a Kalman-filter-based real-time precise orbit determination and the results are compared to a precise reference trajectory for the LEO satellite. The performance of the simulated GPS-only POD is compared to complementary results obtained with real flight-data of Swarm-C to confirm that the simulated data properly reflect the tracking performance of a spaceborne GNSS receiver.

For GPS-based navigation, a very similar performance is found for use of legacy P(Y) and new L2C signals. Even though L2C and the CNAV navigation message are only transmitted by part of the full constellation so far, the number of L2C-capable satellites has grown sufficiently to enable competitive navigation accuracy with purely civil dual-frequency signals. Given the long lead time in space mission and spaceborne GNSS receiver design, it appears safe at this stage to drop support of semi-codeless P(Y) tracking in these applications.

Comparing the performance of individual GNSSs, the study results show that the new Galileo and BeiDou-3 systems offer best prospects for precise onboard orbit determination based on broadcast ephemerides. Using either of these constellations, a 3D position accuracy close to one decimeter can be obtained in a navigation filter processing dual-frequency pseudorange and carrier-phase observations with a high-fidelity reduced dynamic orbit model. Even though the signal modulations of Galileo and BeiDou-3 open service signals outperform GPS in terms of measurement noise and multipath, the low signal-in-space range error of these constellations can be identified as the key factor for the superior navigation accuracy. Compared to GPS-standalone navigation, a 2 to 3-fold improvement may be noted. In view of common frequency bands and interoperable signals, GPS and BeiDou-3 can also favorably be tracked together and combined in a dual-constellation navigation filter. Aside from increased robustness and redundancy, a further reduction of the 3D rms position error to less than 10 cm is achieved. For the triple constellation no further benefit has been obtained, though, that would justify the increased resource requirements in terms of GNSS hardware and computational resources.

The findings show that use of (near) real-time corrections for rapid precise orbit determinations of LEO satellites has largely become dispensable thanks to the high quality of broadcast ephemerides in the new constellations. Precise orbit information can now be made available on board in real-time without a need for complementary ground-to-space links. This represents a paradigm change and allows for an increased shift of science data processing from ground facilities to onboard systems. Beneficiaries of this evolution may include not only altimetry missions and upcoming nano-satellite constellations for remote sensing of the atmosphere, but also GNSS overlay systems transmitting navigation signals from a fleet of LEO satellites.

ACKNOWLEDGEMENTS

Open access funding enabled and organized by Projekt DEAL.

ORCID

André Hauschild https://orcid.org/0000-0002-0172-3492
Oliver Montenbruck https://orcid.org/0000-0003-4783-745X

REFERENCES

Agrotis, L., Schönemann, E., Enderle, W., Caissy, M., & Rülke, A. (2017). The IGS real time service. In M. Mayer, & A. Born (Eds.), *Proc. DVW Seminar "GNSS 2017 – Kompetenz für die Zukunft", 21-22 Feb. 2017, Potsdam*, 121–131. DVW – Gesellschaft für Geodäsie, Geoinformation und Landmanagement e.V.

Andres, Y., Righetti, P. L., & Marquardt, C. (2010). Near real time precise orbit determination for radio occultation and altimetry missions. *Proc. of the 23rd International Technical Meeting of the Satellite Division of The Institute of Navigation (ION GNSS 2010), Portland, Oregon* 2695–2705.

Anthes, R. A. (2011). Exploring earth's atmosphere with radio occultation: contributions to weather, climate and space weather. *Atmospheric Measurement Techniques*, *4*(6), 1077–1103.

Betz, J. (2016). *Engineering satellite-based navigation and timing – Global Navigation Satellite Systems, Signals, and Receivers*. Wiley-IEEE Press.

CDDIS (2020). Crustal dynamics data information system. https://cddis.nasa.gov/archive/.

Desai, S. D., & Haines, B. J. (2010). Precise near-real-time sea surface height measurements from the Jason-1 and Jason-2/OSTM missions. *Marine Geodesy*, *33*(S1), 419–434.

Dilssner, F. (2010). GPS IIF-1 satellite antenna phase center and attitude modeling. *Inside GNSS*, *5*(6), 59–64.

Dilssner, F., Laufer, G., Springer, T., Schonemann, E., & Enderle, W. (2018). The Beidou attitude model for continuous yawing MEO and IGSO spacecraft. In *EGU 2018*.

ESA (2020). Earth Online – Swarm data access. https://earth.esa.int/web/guest/swarm/data-access.

Fernández-Hernández, I., Vecchione, G., Diaz-Pulido, F., Jeannot, M., Valentaite, G., Blasi, R., Reyes, J., & Simón, J. (2018). Galileo high accuracy: A program and policy perspective. In *Proc. Int. Astronaut. Congr. (IAC)*. IAC 18-B2.4.1.

Giordano, P., Zoccarato, P., Otten, M., & Crisci, M. (2017). P2OD: Real-time precise onboard orbit determination for LEO satellites. *Proc. of the 30th International Technical Meeting of the Satellite Division of The Institute of Navigation (ION GNSS+ 2017), Portland, Oregon* 1754–1771. https://doi.org/10.33012/2017.15190.

Gong, X., Guo, L., Wang, F., Zhang, W., Sang, J., Ge, M., & Schuh, H. (2019). Precise onboard real-time orbit determination with a low-cost single-frequency GPS/BDS receiver. *Remote Sensing*, *11*(11), 1391.

Gong, X., Sang, J., Wang, F., & Li, X. (2020). LEO Onboard Real-Time Orbit Determination Using GPS/BDS Data with an Optimal Stochastic Model. *Remote Sensing*, *12*(20), 3458.

Gruber, B. (2010). Global positioning systems wing. *Proc. of the 23rd International Technical Meeting of the Satellite Division of The Institute of Navigation (ION GNSS 2010), Portland, Oregon*, 590–608.

GSC (2019). Galileo satellite metadata website, Galileo Service Center. https://www.gsc-europa.eu/support-to-developers/galileo-iov-satellite-metadata, last updated April 2019.

Gunning, K., Blanch, J., & Walter, T. (2019). SBAS corrections for PPP integrity with solution separation. *Proc. of the 2019 International Technical Meeting (ITM 2019) of The Institute of Navigation, Reston, Virginia*, 707–719. https://doi.org/10.33012/2019.16739.

Hadas, T., Kazmierski, K., & Sośnica, K. (2019). Performance of Galileo-only dual-frequency absolute positioning using the fully serviceable Galileo constellation. *GPS Solutions*, *23*(4), 108.

Haddad, R., Kovach, K., Slattery, R., & Gillis, J. (2020). GPS Modernization and Beyond. In *IEEE/ION Position, Location and Navigation Symposium (PLANS)*, 399–406.

Hairer, E., Nørsett, S. P., & Wanner, G. (1987). *Solving ordinary differential equations I. Nonstiff problems*. Springer.

Harris, I., & Priester, W. (1962). Time-dependent structure of the upper atmosphere. NASA 87-FM-2, Goddard Space Flight Center, MD.

Hauschild, A. (2017). Basic observation equations. In P. Teunissen, & O. Montenbruck (Eds.), *Springer handbook of global navigation satellite systems*, 561–582. Springer.

Hauschild, A., & Montenbruck, O. (2020). Precise On-Board Navigation of LEO Satellites with GNSS Broadcast Ephemerides. *Proc. of the 33rd International Technical Meeting of the Satellite Division of The Institute of Navigation (ION GNSS+ 2020)*, 3866–3874. https://doi.org/10.33012/2020.17752.

Hauschild, A., Tegedor, J., Montenbruck, O., Visser, H., & Markgraf, M. (2016). Precise onboard orbit determination for LEO satellites with real-time orbit and clock corrections. *Proc. of the 29th International Technical Meeting of the Satellite Division of The Institute of Navigation (ION GNSS+ 2016), Portland, Oregon*, 3715–3723. https://doi.org/10.33012/2016.14717.

Heckler, G. W., Gramling, C., Valdez, J., & Baldwin, P. (2016). TDRSS augmentation service for satellites. In *14th International Conference on Space Operations*. AIAA. 2016-2467.

IGS/RTCM (2019). RINEX – the receiver independent exchange format, v.3.04, update 1. 26 April 2019; IGS RINEX Working Group and RTCM-SC104.

Jayles, C., Chauveau, J. P., & Rozo, F. (2010). DORIS/Jason-2: better than 10 cm on-board orbits available for near-real-time altimetry. *Advances in Space Research*, *46*(12), 1497–1512.

Johnston, G., Riddell, A., & Hausler, G. (2017). The International GNSS Service. In P. Teunissen, & O. Montenbruck (Eds.), *Springer Handbook of Global Navigation Satellite Systems*, 967–982. Springer.

Kechine, M., Tiberius, C., & Van der Marel, H. (2004). An experimental performance analysis of real-time kinematic positioning with NASA's internet-based global differential gps. *GPS Solutions*, *8*(1), 9–22.

Kim, J., & Kim, M. (2018). Orbit determination of low-earth-orbiting satellites using space-based augmentation systems. *Journal of Spacecraft and Rockets*, *55*(5), 1300–1302.

Kouba, J. (2009). A simplified yaw-attitude model for eclipsing GPS satellites. *GPS Solutions*, *13*(1), 1–12.

Kursinski, E. R., Hajj, G. A., Schofield, J. T., Linfield, R. P., & Hardy, K. R. (1997). Observing earth's atmosphere with radio occultation measurements using the Global Positioning System. *Journal of Geophysical Research*, *102*(D19), 23429–23465.

Lear, W. M. (1989). GPS navigation for low-Earth orbiting vehicles. NASA 87-FM-2, JSC-32031, rev. 1, Lyndon B. Houston, TX: Johnson Space Center.

Mao, X., Visser, P., & van den IJssel, J. (2018). The impact of gps receiver modifications and ionospheric activity on swarm baseline determination. *Acta Astronautica*, *146*, 399–408.

Marquis, W. A., & Reigh, D. L. (2015). The GPS Block IIR and IIR-M broadcast L-band antenna panel: Its pattern and performance. *NAVIGATION*, *62*, 329–347.

Monjas, F., Montesano, A., & Arenas, S. (2010). Group delay performances of Galileo system navigation antenna for global positioning. In *Proc. 32nd ESA Antenna Workshop on Antennas for Space Applications*. ESA.

Montenbruck, O., & Gill, E. (2000). *Satellite orbits*. Springer.

Montenbruck, O., Hackel, S., van den Ijssel, J., & Arnold, D. (2018a). Reduced dynamic and kinematic precise orbit determination for the Swarm mission from 4 years of GPS tracking. *GPS Solutions*, *22*(3), 79.

Montenbruck, O., Hauschild, A., Andres, Y., von Engeln, A., & Marquardt, C. (2013). (Near-) real-time orbit determination for GNSS radio occultation processing. *GPS Solutions*, *17*(2), 199–209.

Montenbruck, O., Markgraf, M., Naudet, J., Santandrea, S., Gantois, K., & Vuilleumier, P. (2008). Autonomous and precise navigation of the PROBA-2 spacecraft. In *AIAA/AAS Astrodynamics Specialist Conference and Exhibit* (pp. 3715–3723).

Montenbruck, O., & Ramos-Bosch, P. (2008). Precision real-time navigation of LEO satellites using global positioning system measurements. *GPS Solutions*, *12*(3), 187–198.

Montenbruck, O., Steigenberger, P., & Hauschild, A. (2018b). Multi-GNSS signal-in-space range error assessment – methodology and results. *Advances in Space Research*, *61*(12), 3020–3038.

Moreau, M. C., Davis, E. P., Carpenter, J. R., Kelbel, D., Davis, G. W., & Axelrad, P. (2002). Results from the GPS flight experiment on the high earth orbit AMSAT OSCAR-40 spacecraft. *Proc. of the 15th International Technical Meeting of the Satellite Division of The Institute of Navigation (ION GPS 2002), Portland, Oregon*, 122–133.

Petovello, M. G., & Curran, J. T. (2017). Simulators and test equipment. In P. Teunissen, & O. Montenbruck (Eds.), *Springer Handbook of Global Navigation Satellite Systems*, (chapter 18, 535–558. Springer.

Reichert, A., Meehan, T., & Munson, T. (2002). Toward decimeter-level real-time orbit determination: a demonstration using the SAC-C and CHAMP spacecraft. *Proc. of the 15th International Technical Meeting of the Satellite Division of the Institute of Navigation (ION GPS 2002), Portland, Oregon*, 1996–2003.

Rizos, C., & Stolz, A. (1985). Force modelling for GPS satellite orbits. *Proc. 1st Int. Sym. Precise Positioning with GPS*, Rockville, MD, volume *1*, 87–98.

Roselló, J., Silvestrin, P., Weigand, R., d'Addio, S., Rodríguez, A. G., & Risueño, G. L. (2012). Next generation of ESA's GNSS receivers for earth observation satellites. *Proc. 6th ESA Workshop on Satellite Navigation Technologies (Navitec 2012)*, 3715–3723.

Steigenberger, P., Thoelert, S., & Montenbruck, O. (2018). GNSS satellite transmit power and its impact on orbit determination. *Journal of Geodesy*, *92*(6), 609–624.

Steigenberger, P., Thölert, S., & Montenbruck, O. (2019). Flex power on GPS Block IIR-M and IIF. *GPS Solutions*, *23*(1), 8.

Tapley, B. D., Bettadpur, S., Watkins, M., & Reigber, C. (2004). The gravity recovery and climate experiment: Mission overview and early results. *Geophysical Research Letters*, *31*(9).

Toral, M., Stocklin, F., Bar-Server, Y., Young, L., & Rush, J. (2006). Extremely accurate on-orbit position accuracy using NASA's tracking and data relay satalite system (TDRSS). In *Proc. 24th AIAA Int. Communications Satellite Systems Conference (ICSST)*. 2006-5312.

Valle, P., Netti, A., Zolesi, M., Mizzoni, R., Bandinelli, M., & Guidi, R. (2006). Efficient dual-band planar array suitable to Galileo. In *Proc. 1st EUCAP 2006*. IEEE.

van den IJssel, J., Encarnação, J., Doornbos, E., & Visser, P. (2015). Precise science orbits for the Swarm satellite constellation. *Advances in Space Research*, *56*(6), 1042–1055.

Wang, F., Gong, X., Sang, J., & Zhang, X. (2015). A novel method for precise onboard real-time orbit determination with a standalone GPS receiver. *Sensors*, *15*(12), 30403–30418.

Wettergren, J., Bonnedal, M., Ingvarson, P., & Wästberg, B. (2009). Antenna for precise orbit determination. *Acta Astronautica*, *65*(11-12), 1765–1771.

Woo, K. T. (2000). Optimum semicodeless carrier-phase tracking of L2. *NAVIGATION*, *47*, 82–99.

Wu, J. T., Wu, S. C., Hajj, G. A., Bertiger, W. I., & Lichten, S. M. (1993). Effects of antenna orientation on GPS carrier phase. *Manuscripta Geodaetica*, *18*(2), 91–98.

Zangerl, F., Griesauer, F., Sust, M., Montenbruck, O., Buchert, B., & Garcia, A. (2014). SWARM GPS precise orbit determination receiver initial in-orbit performance evaluation. In *Proc. of the 27th International Technical Meeting of the Satellite Division of The Institute of Navigation (ION GNSS+ 2014), Tampa, Florida*, 1459–1468.

Zhan, X., Jing, S., & Wang, X. (2013). Beidou space service volume parameters and its performance. In *Proc. 8th meeting of the International Committee on GNSS*.

How to cite this article: Hauschild A, Montenbruck O. Precise real-time navigation of LEO satellites using GNSS broadcast ephemerides. *NAVIGATION*. 2021;1–14.
https://doi.org/10.1002/navi.416